Proc. Natl. Acad. Sci. USA
Vol. 78, No. 5, pp. 2947–2951, May 1981
Biophysics

Location of platinum binding sites on bacteriorhodopsin by electron diffraction

(electron crystallography/purple membrane/isomorphous replacement/*Halobacterium halobium*/glycyl-L-methionatoplatinum)

MARK E. DUMONT*, J. W. WIGGINS*, AND S. B. HAYWARD†‡

*Department of Biophysics, The Johns Hopkins University, Baltimore, Maryland 21218; and †Division of Medical Physics, Graduate Group in Biophysics and Donner Laboratory, University of California, Berkeley, California 94720

Communicated by William F. Harrington, January 16, 1981

ABSTRACT **A platinum-containing derivative of bacteriorhodopsin has been prepared by treating purple membranes with glycyl-L-methionatoplatinum. Low-dose electron diffraction was used to identify Pt binding sites in the 5.6 Å resolution reconstruction of the bacteriorhodopsin unit cell in projection. This is a necessary first step in the use of the Pt derivative for identifying the parts of the amino acid sequence corresponding to the α helices in the bacteriorhodopsin structure and for obtaining phases for reflections out to 3.5 Å resolution by the method of heavy-atom isomorphous replacement. The largest peak in a Fourier difference map between platinum-labeled and native purple membrane is larger than the spurious features expected to arise from errors in measurements of diffraction intensities.**

A number of proteins that have biologically interesting functions have been found to be capable of forming two-dimensional crystalline arrays, but not, as of yet, well-ordered three-dimensional crystals (1–6). Electron diffraction and electron imaging have been used in the structural analyses of these proteins because of the difficulty of obtaining single-crystal x-ray diffraction patterns from two-dimensional small crystals. We discuss here the use of single heavy-atom labels for obtaining detailed structural information from two-dimensional arrays, using as a demonstration our studies of Pt binding to bacteriorhodopsin (BR), the light-driven proton pump from the purple membrane fraction of *Halobacterium halobium*.

The tendency of BR to form two-dimensional crystals allowed Henderson and Unwin to use low-dose electron imaging and diffraction to determine the three-dimensional structure of the molecule to 7 Å resolution (1, 7). Two main factors have blocked the extension of this structural study to higher resolution. First, it has been difficult to obtain significant intensity in high-resolution diffraction orders. Because purple membranes are ordered to at least 3.5 Å resolution (8), intensity is limited by the low levels of electron irradiation that can be tolerated without destruction of the specimen and by the small size of the crystalline membrane patches. Second, currently available electron imaging systems are incapable of achieving 3.5 Å resolution over large specimen areas without distortion (9).

As the amino acid sequence of BR is known (10, 11), one way to get a detailed understanding of BR chain folding is to attach heavy atoms to known amino acids in the sequence and use electron diffraction to locate the heavy atoms in the low-resolution structure. The high α helix content of the protein has already led to some model building efforts (12), a major remaining uncertainty being the question of which part of the sequence is identified with each α helical segment in the structural map.

Recently, Hayward and Glaeser (13) demonstrated a significant improvement in the radiation resistance of BR when the specimen is maintained at −120°C during the exposure to electrons. This result, combined with the use of high-speed photographic emulsions, has allowed the collection of diffraction intensities from single crystals out to 2.65 Å resolution. Thus, for data from 6 to 3 Å, there remains a phase problem similar to that encountered in x-ray crystallography. Heavy-atom labeling may prove useful in determining the missing phases by a technique analogous to the x-ray method of multiple isomorphous replacement.

In the use of heavy-atom labels, either for locating particular segments of the sequence in the low-resolution structure or for determining the phases of the high-resolution reflections, the first step is the location of the sites of binding in the unit cell. We report here a reliable identification of a single heavy-atom binding site in a protein by electron crystallography, emphasizing the adaptations of x-ray crystallographic techniques that proved useful in our analysis. The small number of unit cells contributing to the purple membrane diffraction patterns and the weakness of the heavy-atom component of the electron scattering made it essential to carefully evaluate the statistical significance of the results.

Biochemical studies suggesting that the Pt binds primarily to methionine residues in BR have been reported in preliminary form (14).

MATERIALS AND METHODS

Purple membranes were isolated (15) from the strain S9 of *Halobacterium halobium*, obtained from the laboratory of Walther Stoeckenius. Membranes were stored in 10 mM phosphate buffer, pH 6.9/5 mM sodium azide until used.

Pt Binding. The labeling reagent used was the dark form of a complex between the dipeptide glycyl-L-methionine and Pt (16). The structure of a related compound is known (17). The resinous product (Gly-Met–Pt) of the synthesis was solubilized for reaction with purple membranes by placing it in 1 M NaOH, and this solution was then titrated to the reaction pH with HCl and diluted with buffer.

The Gly-Met–Pt purple membrane reaction was carried out at pH 6.9 in sodium phosphate buffer. Reaction mixtures were ≈20 μM in BR and contained an 80-fold molar excess of Pt to BR.

Pt binding to BR was assayed in aliquots from the reaction mixture. Samples were washed twice by centrifuging for 15 min in a Beckman Type 65 rotor at 40,000 rpm to remove free Pt.

The publication costs of this article were defrayed in part by page charge payment. This article must therefore be hereby marked "*advertisement*" in accordance with 18 U. S. C. §1734 solely to indicate this fact.

Abbreviations: BR, bacteriorhodopsin; Gly-Met–Pt, glycyl-L-methionatoplatinum.

‡ Present address: California State Dept. of Health, 2151 Berkeley Way, Berkeley, CA 94704

The Pt concentration was measured by the method of Ayers and Meyer (18), except that the protein was hydrolyzed overnight in 2 M HCl/2.5% H_2O_2 at 100°C before the other reagents were added. The H_2O_2 was used to remove interference from free retinal in the spectrophotometric measurement. A correction was made for scattering from white specks, presumably lipid, that appeared in the hydrolyzed samples and for the small remaining amount of unbleached retinal.

Protein concentrations in aliquots from the reaction mixtures were measured using an extinction coefficient for BR of 63,000 liter mol^{-1} cm^{-1} at 568 nm (19) and applying a correction factor for scattering by the membrane patches. The correction was based on the measured scattering at 750 nm and was assumed proportional to λ^{-2}.

Electron Diffraction. Labeled specimens used for diffraction were incubated with Gly-Met–Pt for 1 week, washed twice with phosphate buffer, and checked for Pt uptake. Labeled and unlabeled specimens were suspended in buffer and mixed with an equal volume of 2% glucose and 0.02% sodium azide. A drop was placed on a grid covered with a thin carbon film on gold holey film, extra moisture was blotted off, and the grid was dried in air.

Electron diffraction was performed using a cold stage on a JEOL 100B (13). A field-limiting aperture was used to select a 0.75- or 1.25-μM-diameter area on the specimen. The electron dose to the specimen during diffraction was either one or two electrons per Å^2. Patterns were recorded on glass plates coated with Kodak NTB2 emulsions (20). Development was in fresh D19 developer for 18 min at 20°C. Each set of plates that was processed included calibrations of optical density versus electron flux in which plates were exposed to the same beam spot for various lengths of time. A Si(Li) detector below the viewing plane allowed calibration of electron doses.

Diffraction patterns were digitized on a Perkin Elmer PDS 1010A microdensitometer. Scanning rasters ranged from 6 to 12 μM, with the largest rasters used only for digitizing patterns with average spot half-widths greater than 100 μM.

Initial processing made use of a PDP11/20 computer with a display system (21). Spot locations relative to the microdensitometer raster were fit to a lattice by using a third-order least-squares procedure in two dimensions. A second least-squares routine fit the standard dose–density calibration for each set of patterns to the theoretical form for such curves (22). In some cases, this was indistinguishable from linearity over the range of measured densities.

Diffraction intensities were determined by summing the number of electrons striking each of the picture elements in a diffraction spot. Background corrections, calculated by averaging the electron dose in a ring around a given spot and multiplying that average by the number of picture elements in a spot, were subtracted from the integrated intensities. Integrations were made over different spot sizes for each diffraction pattern and then averaged together.

Before averaging, all data sets were adjusted by a modified "Wilson scaling" technique to minimize differences in average intensity and apparent temperature factor. A least-squares program fit the ratio of the intensities of two data sets to be averaged to a function of the form $A\ exp(-B\theta^2)$. One of the data sets was then adjusted so as to make $A = 1$ and $B = 0$. In the final averaging, different data sets were weighted by the reciprocal of their symmetry R values (to 7 Å resolution), except that one pattern, more tilted than the others, was weighted by 80% of the reciprocal of its R value.

Phases for native membrane structure factors were determined (23) from computer-generated Fourier transforms of low-dose electron images of purple membranes recorded on a liquid nitrogen-cooled specimen stage. The peak to background ratio and the uncertainty in the contrast transfer function at each point on the reciprocal lattice were used to weight individual measurements in averaging the transforms from different membrane images by generating a probability distribution for each phase similar to that commonly used by x-ray crystallographers (24). This allowed calculation of a "best" phase and a "figure of merit" (25) for each reflection. The mean figure of merit of this phase determination to 5.6 Å was 0.95. The mean difference between these phases and those determined to 7 Å by Unwin and Henderson is 20°, with better agreement for the stronger reflections. Maps generated by using the amplitudes given in this paper and the phases of Unwin and Henderson show the same general features as Figs. 2 and 3.

Image reconstruction was performed on an IBM 360/91 using the Basel image processing system (26).

RESULTS

Gly-Met–Pt Binding to BR. Gly-Met–Pt labeling of BR caused no drastic alterations in the state of the membrane patches, as judged by dark-field electron microscopy, preservation of crystalline order, and the shape of the absorption spectrum. Although the labeled patches showed some tendency to aggregate, this was slight compared with the effects of other labeling compounds that were tried. Filtering to remove aggregates from suspensions before chemical analysis caused no change in the results of the Pt determinations.

The binding of Gly-Met–Pt to BR shows an initial fast component, followed by a slower increase with time (Fig. 1). Although it was difficult to obtain completely reproducible amounts of binding, most determinations showed two or three Pt atoms per BR after 1 week. The extent of binding is affected by salt concentration and temperature and is a strong function of pH. The Pt–protein complex was stable over at least several days in phosphate buffer (see Fig. 1).

Diffraction. Both native and Pt-labeled purple membranes were found to be ordered to at least 3.5 Å resolution and showed similar apparent temperature factors. However, for reasons discussed below, we found errors in our measurements that are very large by conventional x-ray crystallographic standards.

A labeled-native Fourier difference map (in projection) to 5.6 Å was prepared (Fig. 2) based on the averages of eight native and five labeled membranes (see Table 1). Such a map is a Fourier synthesis of the scalar amplitude differences between native and labeled membrane diffraction patterns, with the phases of the native membranes. The labeled membrane amplitudes

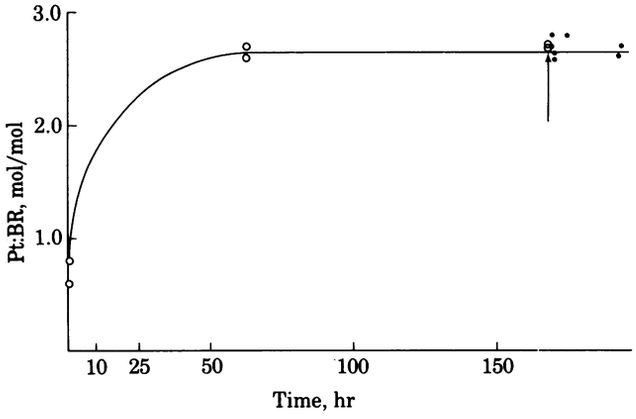

FIG. 1. Gly-Met–Pt binding to BR. At the time indicated by the arrow, the BR was spun out of the Pt solution.

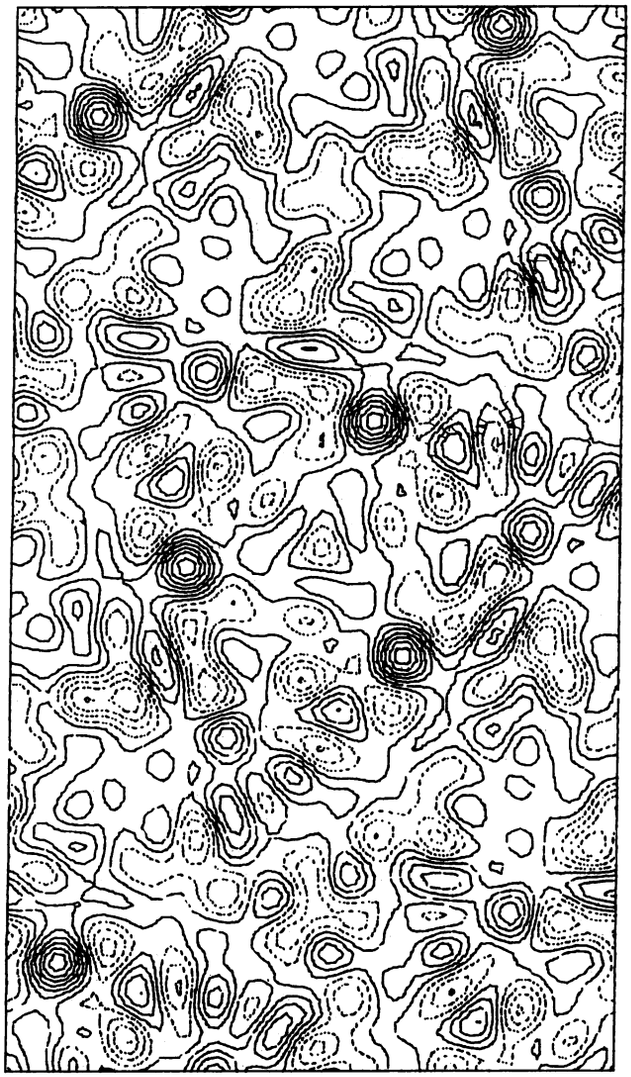

FIG. 2. Fourier difference map. The map is synthesized from the phases determined (unpublished results) and the measured differences in amplitude between labeled and unlabeled membrane diffraction patterns. Dashed contours are negative. The lowest solid contour is at zero density. Total range of the map is ≈8% of that in Fig. 3.

were scaled to be 1.018 times greater than the native membrane amplitudes over all reciprocal space to allow for scattering from the Pt (though the appearance of the maps was not sensitive to the exact scaling used). The (1,0), (6,3), and (5,6) reflections were omitted from the synthesis because they were usually much smaller than the background fluctuations in their regions of reciprocal space.

The most positive peak in Fig. 2 is about 1.4 times the magnitude of the deepest negative peak, with the total relief of the difference map spanning only 8% of the range of densities in the native membrane map (Fig. 3).

DISCUSSION

Statistical Uncertainties in Electron Crystallography. The symmetry R values[§] of the individual membrane diffraction patterns described here ranged from 16% to 25% (out to 7 Å resolution, neglecting reflections considered to be less than twice the measured background fluctuations). Such R values are much higher than the 5% usually considered acceptable for x-ray crystallography (26), indicating poor agreement between symmetry-related reflections. There are at least four likely sources for the discrepancies in these intensity measurements. (*i*) Statistical fluctuations in the number of electrons in a diffraction spot and its background: A typical diffraction reflection (at less than 5.6 Å resolution) is made up of ≈200 electrons striking the plate. At least several times this number of electrons, scattered inelastically off the BR crystal or striking disordered parts of the specimen, form a diffuse background upon which the coherently diffracted electrons are superimposed. Thus, the statistical uncertainty in diffraction intensity is actually of two types, the first stemming from fluctuations in the total number of electrons making up the reflection and the second from the uncertainty in calculating the background correction. If the distribution of numbers of electrons per diffraction spot is assumed to obey Poisson statistics, these effects alone lead us to expect symmetry R values on the scale of those that we have observed. (*ii*) Microdensitometer errors: Two separate scans of the same diffraction pattern gave R values of 2% or 3% when symmetry averaged intensities were compared. (*iii*) Uncertainty in relating electron dose to film density: Although it was possible to compensate for variations in the dose–density response of batches of plates, even individual plates exhibited variations in speed and fog level. (*iv*) Undesired tilting of the specimen: Because the intensities of some reflections vary strongly with tilt angle, it is possible to select untilted diffraction patterns. All but one of those included in the final averaging had tilts of no more than a few degrees.

The uncertainty indicated by the 20% symmetry R factor can

Table 1. Diffraction amplitudes for native and Pt-labeled purple membrane diffraction patterns (scaled 1:1)

	Amplitude			Amplitude	
(*h*,*k*)	Native	Labeled	(*h*,*k*)	Native	Labeled
(1,1)	65.07	65.56	(5,5)	11.30	7.96
(2,0)	47.91	45.18	(6,0)	38.27	38.69
(2,1)	23.09	17.81	(6,1)	44.67	47.41
(1,2)	38.75	33.56	(1,6)	13.75	9.78
(2,2)	47.63	50.78	(6,2)	19.48	18.23
(3,0)	20.31	15.92	(2,6)	26.89	25.07
(3,1)	59.21	57.39	(3,6)	12.84	10.87
(1,3)	18.25	15.92	(6,4)	16.24	17.00
(3,2)	45.71	44.57	(4,6)	9.89	11.04
(2,3)	31.11	28.97	(6,5)	11.96	9.47
(3,3)	14.27	11.66	(7,0)	28.31	32.82
(4,0)	46.32	44.51	(7,1)	31.89	31.81
(4,1)	57.54	58.35	(1,7)	42.06	45.51
(1,4)	49.78	48.22	(7,2)	11.53	13.03
(4,2)	34.44	32.06	(2,7)	23.91	24.89
(2,4)	75.77	76.31	(7,3)	18.27	15.41
(4,3)	86.46	91.55	(3,7)	24.04	21.81
(3,4)	54.14	52.84	(7,4)	9.39	7.81
(4,4)	19.25	19.36	(4,7)	10.83	13.43
(5,0)	61.84	64.39	(8,0)	10.88	10.53
(5,1)	16.68	18.02	(8,1)	10.45	9.57
(1,5)	55.17	53.82	(1,8)	14.27	14.72
(5,2)	54.13	57.88	(8,2)	17.25	18.45
(2,5)	21.21	22.12	(2,8)	30.66	27.02
(5,3)	17.68	19.00	(9,0)	9.97	13.14
(3,5)	50.07	50.77	(9,1)	24.94	25.41
(5,4)	11.77	9.04	(1,9)	17.11	15.21
(4,5)	19.87	20.29			

[§] $R_s = \Sigma_h|I_h - \bar{I}|/\Sigma_h I_h$, where the summation is over all reflections, I_h is the intensity of each reflection, and $\bar{I}$ is the average of the symmetry set to which a reflection belongs.

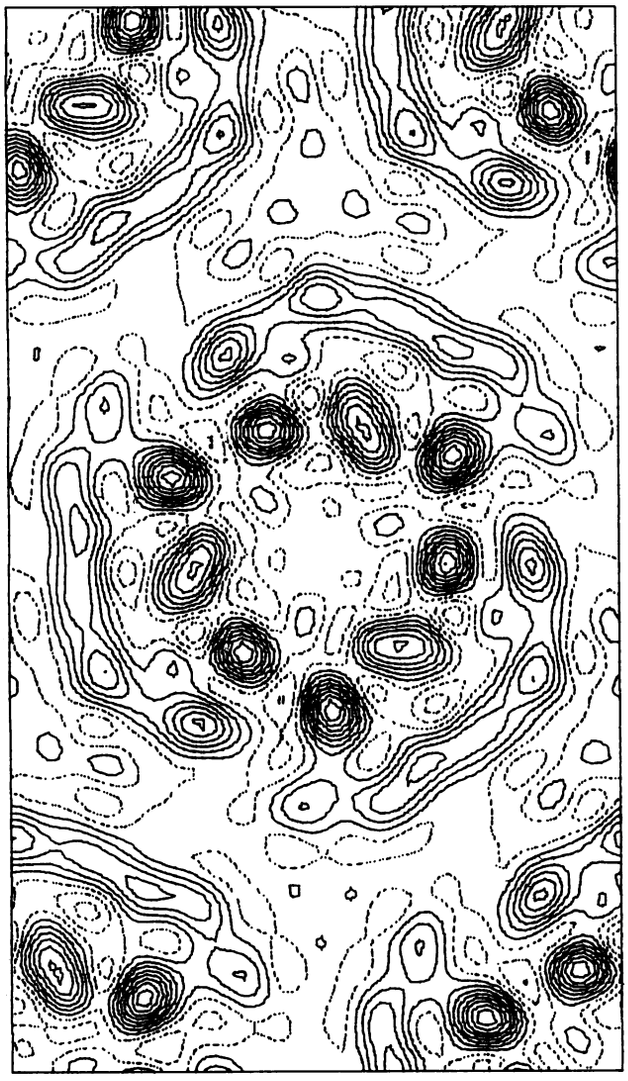

FIG. 3. Unlabeled purple membrane (in projection) map synthesized from amplitudes measured in this work and phases as in Fig. 2.

be propagated through the rest of our calculations to give estimated errors close to those that we actually observe. For instance, six-fold averaging of intensities in a single pattern should reduce the error by a factor of $\sqrt{6}$. This is consistent with the $\approx$9% intensity R value[¶] that is observed in comparing individual diffraction patterns, indicating that it is possible to deal with the discrepancies between patterns by averaging large amounts of data.

The details of the scaling and averaging techniques used in combining diffraction patterns have turned out to be quite important. Initial attempts at scaling in which the actual diffraction intensities (rather than the ratios of intensities from different diffraction patterns) were fitted to multiplicative and exponential factors gave results somewhat different from those reported here. The scaling procedure used in generating the results shown in Fig. 2 took into account the statistical uncertainty in the intensities by weighting the least-squares terms of the modified Wilson scaling by the reflection intensity. This kept the fitting from being overly influenced by the small reflections for which the uncertainty in the ratio of intensities is large.

[¶] $R = \Sigma|I_1 - I_2|/\Sigma(I_1 + I_2)$, where I_1 and I_2 are the corresponding symmetry-averaged reflections in the two data sets being compared and the summation is over all symmetry-averaged reflections.

Most systematic errors in this analysis should not significantly affect the results because of the identical treatment of data from labeled and native membranes. There remains the unlikely possibility that there is some difference between the radiation sensitivities of the native and the labeled membranes. However, given the gentleness of the Pt reaction, such a change in radiation sensitivity would most likely result from liberation of the bound Pt. This would simply show up as a decrease in the size of the Fourier difference map peaks. A less likely possibility is some disruption of molecular structure immediately adjacent to the Pt binding site. In this case, the locations of the peaks could still shed light on the whereabouts of the Pt binding.

Statistical Significance of the Maps. A fundamental problem in evaluating the maps presented here is that of determining whether the presumptive Pt sites are real or whether they result from Fourier transforming the errors in the diffraction amplitudes.

When the individual diffraction patterns from native (or labeled) membranes are arbitrarily partitioned into two groups and the intensities from one such half data set are compared with those from the other independent half data set, intensity R values of 4% or 5% are obtained. This uncertainty in the intensities would be expected to decrease by a factor of $\sqrt{2}$ when the half data sets of each type are averaged together. When the entire labeled data set is compared with the entire native data set, with the two scaled by our modified Wilson scaling procedure to be as similar as possible, the intensity R value is 5%. Thus, the difference between the labeled and native intensities is greater than the error in the averaged native or labeled intensities, indicating a real change in diffraction caused by Pt binding. Even a difference in intensity of the same magnitude as the uncertainty in intensity could show up as a significant feature in the difference map, because the differences corresponding to real features should add coherently in the Fourier synthesis, whereas differences caused by random errors should add incoherently.

We have generated Fourier difference maps in which half the diffraction patterns from labeled (or native) membranes are compared with the other independent half. In such maps, the peaks and valleys are about the same distances above and below zero and the total range of the maps is slightly less than the range of the labeled-native Fourier difference maps. As above, on averaging the final half data sets of each type together, the peak-to-peak range of the noise features in these "error" maps should decrease by $\approx\sqrt{2}$. Thus, the range of densities in the labeled-native Fourier difference map is about $\sqrt{2}$ times the expected peak-to-peak noise, indicating that there are statistically significant features in the map.

X-ray crystallographers have developed and tested methods for evaluating the significance of peaks in Fourier difference maps (27, 28). Using the technique of Henderson and Moffat (27, 28), estimating the errors in the amplitude measurements from the discrepancies between independent half data sets (see above), and neglecting the small errors in the native protein phases, we find that the largest positive peak in the Fourier difference map is 3.7 times the estimated rms error in the map. This is a significant result by Henderson and Moffat's criteria. The deepest negative valley in the map is 2.7 times the expected rms error.

Because we have not included the (0,0) reflection in any of these calculations, the average integrated intensity of the difference map must be zero. Thus, if we are to have positive peaks in the Fourier difference map, they must rise above a background that has a negative average value. Such a negative background will fluctuate farther into negative densities than it does into positive densities. Thus, it is possible for a difference map with no larger positive than negative densities to contain sta-

tistically significant heavy atom positions. We have verified, by using calculated heavy-atom structure factors, that the assumptions involved in making Fourier difference maps can, in the absence of an amplitude for the (0,0) reflection, lead to large negative peaks in such difference maps.

Using the estimated peak-to-peak noise in the labeled-native Fourier difference map and assuming that the noise fluctuates symmetrically above and below the background, we can estimate the "true" background level in the difference map. Measured from this level, the highest peak in the difference map is ≈4.1 times the expected rms error in the map calculated by the technique of Henderson and Moffat (28). The second highest peak in the Fourier difference map is 3.0 times the expected rms noise in the map, ≈70% of the density of the strongest peak.

The ratio of the peak positive density in the Fourier difference map (see Fig. 2) to the density of a feature representing an alpha helix viewed end-on in the membrane reconstruction is about half that expected for a Pt atom at 100% site occupancy. Noise in the diffraction amplitudes has the effect of reducing the intensity of the Pt peak.

A Patterson difference map (not shown) (27) was prepared, based on the intensities of the native and labeled membrane diffraction to 3.5 Å resolution. This map showed features that were consistent with the Fourier difference map, but the low signal-to-noise ratio created many peaks of similar heights, making it difficult to interpret the Patterson map in the absence of phase information.

The largest peak in the Fourier difference map corresponds to a statistically significant heavy-atom binding site on the most central of the three inner BR alpha helices. If the Engelman *et al.* (12) most likely model is correct, this largest Pt peak would lie on their third transmembrane segment of the polypeptide. Although this segment contains no methionine, the loop connecting the second and third segments in the model contains a methionine that would probably be accessible for labeling. Identification of the exact amino acid residues involved in Gly-Met–Pt binding should allow elimination of the majority of the recently proposed models for BR folding (12).

The number of crystallographically established Pt binding sites on BR is less than the 2.5 determined from chemical binding assays. On the basis of the calculations of the relative scattering of alpha helices and Pt, it is unlikely that our primary peak is due to scattering by two atoms in this site. Thus, either some of the Pt binds to poorly ordered parts of the specimen or some of the binding is not specific, or there are several binding sites that are only partially occupied in the protein. Such low-occupancy sites would not show up as statistically significant peaks in our maps, given the signal-to-noise ratio.

Prospects for Electron Crystallography. Because of the difference in the dependence of scattering power on atomic number of the scattering material for electrons and x-rays (29), heavy atoms cannot be as readily detected by electron-based methods as by x-ray methods. This fact, combined with the low signal-to-noise ratio inherent in low-dose electron diffraction, makes it unlikely that we will be able to arrive at statistically significant phases for more than a few of the high-resolution reflections of native BR. Although it might be possible to achieve greater accuracy by averaging additional large numbers of diffraction patterns, further reduction of the statistical errors would bring them to the magnitude of the errors introduced by the Fourier difference technique, microdensitometer inaccuracies, uncertainty in specimen tilt, and variations in emulsion characteristics. Thus, further averaging may not necessarily improve the significance of the maps.

Our findings raise fundamental concerns about the possibilities for high-resolution structure determination by electron crystallography. For specimens that diffract only as strongly as purple membranes, electron statistics are an inherent limitation on the signal-to-noise ratio. Averaging of independent diffraction data sets is required to achieve accuracy sufficient for locating heavy-atom binding sites. Important gains in signal-to-noise ratios might be achieved by increasing membrane patch (crystal) size or by increasing the dose used in taking the diffraction pattern, perhaps through the use of still lower specimen temperatures to further slow radiation damage.

We gratefully acknowledge advice and support from Michael Beer and Robert Glaeser and helpful discussions with Richard Henderson and Ed Lattman. William Goldfarb assisted in the scanning of the diffraction patterns on the microdensitometer at the New York State Department of Health at Albany. Ross Smith provided the image analysis programs and their excellent documentation. Thea Scott-Garner made the NTB2 plates. This work was supported by Grants 5R01-GM24237 and 5S07-RR07041 from the National Institutes of Health and Grant W-7405-ENG-48 from the U.S. Department of Energy.

1. Henderson, R. & Unwin, P. N. T. (1975) *Nature (London)* **257,** 28–32.
2. Henderson, R., Capaldi, R. A. & Leigh, J. S. (1977) *J. Mol. Biol.* **112,** 631–648.
3. Unwin, P. N. T. & Zampighi, G. (1980) *Nature (London)* **283,** 545–549.
4. dos Remedios, C. G. & Dickens, M. J. (1978) *Nature (London)* **276,** 731–733.
5. Chiu, W. & Hosoda, J. (1978) *J. Mol. Biol.* **122,** 103–107.
6. Ross, M. J., Klymkowsky, M. W., Agard, D. A. & Stroud, R. M. (1977) *J. Mol. Biol.* **116,** 635–659.
7. Unwin, P. N. T. & Henderson, R. (1975) *J. Mol. Biol.* **94,** 425–440.
8. Henderson, R. (1975) *J. Mol. Biol.* **93,** 123–128.
9. Rigden, J. & Wiggins, J. W. (1980) *Proceedings of the 38th Annual Meeting of the Electron Microscopy Society of America,* ed. Bailey, G. W. (Claitor's, Baton Rouge, LA), pp. 684–685.
10. Ovchinnikov, Y. A., Abdulaev, N. G., Feigira, M. Y., Kiselev, A. V. & Lobanov, N. A. (1979) *FEBS Lett.* **100,** 219–224.
11. Khorana, H. G., Gerber, G. E., Herlihy, W. C., Gray, C. P., Anderegg, R. J., Nihei, K. & Biemann, K. (1979) *Proc. Natl. Acad. Sci. USA* **76,** 5046–5050.
12. Engelman, D. M., Henderson, R., McLachlan, A. D. & Wallace, B. A. (1980) *Proc. Natl. Acad. Sci. USA* **77,** 2023–2027.
13. Hayward, S. B. & Glaeser, R. M. (1979) *Ultramicroscopy* **4,** 201–210.
14. Dumont, M. E. & Wiggins, J. W. (1979) *J. Supramol. Struct. Suppl.* **3,** 113.
15. Becher, B. M. & Cassim, J. Y. (1975) *Prep. Biochem.* **5,** 161–178.
16. Mogilevkina, M. F., Revisia, L. B., Rar, V. I., Sekacheva, M. V., Cheremisina, I. M. & Logvinenkov, A. (1976) *Russ. J. Inorg. Chem. (Engl. Transl.)* **21,** 1345–1348.
17. Freeman, H. C. & Golomb, M. L. (1970) *Chem. Commun.* 1523–1524.
18. Ayers, G. H. & Meyer, A. S. (1951) *Anal. Chem.* **23,** 299–304.
19. Rehorek, M. & Heyn, M. P. (1979) *Biochemistry* **18,** 4977–4983.
20. Kuo, I. A. M. & Glaeser, R. M. (1975) *Ultramicroscopy* **1,** 53–66.
21. Zubin, J. A. & Wiggins, J. W. (1980) *Rev. Sci. Instrum.* **51,** 123–131.
22. Valentine, R. C. (1966) in *Advances in Optical and Electron Microscopy,* eds. Barer, R. & Coslett, V. E. (Academic, New York), Vol. 1, pp. 180–203.
23. Hayward, S. B. & Stroud, R. M. (1981) *J. Mol. Biol.*, in press.
24. Blow, D. M. & Crick, F. H. C. (1959) *Acta. Crystallogr. A* **12,** 794–802.
25. Dickerson, R. E., Kendrew, J. C. & Strandberg, B. E. (1961) *Acta. Crystallogr. A* **14,** 1188–1195.
26. Smith, P. R. (1978) *Ultramicroscopy* **3,** 153–160.
27. Blundel, T. L. & Johnson, L. N. (1976) *Protein Crystallography* (Academic, New York).
28. Henderson, R. & Moffat, J. K. (1971) *Acta Crystallogr. B* **27,** 1414–1420.
29. Langmore, J. P., Wall, J. & Isaacson, M. S. (1973) *Optik* **38,** 335–350.